Clim. Past Discuss., 8, 5293–5340, 2012
www.clim-past-discuss.net/8/5293/2012/
doi:10.5194/cpd-8-5293-2012

Climate of the Past Discussions

The last interglacial (Eemian) climate simulated by LOVECLIM and CCSM3

I. Nikolova, Q. Yin, A. Berger, U. K. Singh, and M. P. Karami

George Lemaitre Centre for Earth and Climate Research, Earth and Life Institute, Universite Catholique de Louvain, 3, Place Louis Pasteur, 1348 Louvain-la-Neuve, Belgium

Received: 5 October 2012 – Accepted: 23 October 2012 – Published: 31 October 2012

Correspondence to: I. Nikolova (irina.nikolova@uclouvain.be)

Published by Copernicus Publications on behalf of the European Geosciences Union.

Abstract

This paper presents a detailed analysis of the climate of the last interglacial simulated by two climate models of different complexities, LOVECLIM and CCSM3. The simulated surface temperature, hydrological cycle, vegetation and ENSO variability during the last interglacial are analyzed through the comparison with the simulated Pre-Industrial (PI) climate. In both models, the last interglacial period is characterized by a significant warming (cooling) over almost all the continents during boreal summer (winter) leading to a largely increased (reduced) seasonal contrast in the northern (southern) hemisphere. This is mainly due to the much higher (lower) insolation received by the whole Earth in boreal summer (winter) during this interglacial. The arctic is warmer than PI through the whole year, resulting from its much higher summer insolation and its remnant effect in the following fall-winter through the interactions between atmosphere, ocean and sea ice. In the tropical Pacific, the change in the SST annual cycle is suggested to be related to a minor shift towards an El Nino, slightly stronger for MIS-5 than for PI. Intensified African monsoon and vegetation feedback are responsible for the cooling during summer in North Africa and Arabian Peninsula. Over India precipitation maximum is found further west, while in Africa the precipitation maximum migrates further north. Trees and grassland expand north in Sahel/Sahara. A mix of forest and grassland occupies continents and expand deep in the high northern latitudes. Desert areas reduce significantly in Northern Hemisphere, but increase in North Australia. The simulated large-scale climate change during the last interglacial compares reasonably well with proxy data, giving credit to both models and reconstructions. However, discrepancies exist at some regional scales between the two models, indicating the necessity of more in depth analysis of the models and comparisons with proxy data.

CPD
8, 5293–5340, 2012

1 Introduction

Future climate has long intrigued scientists, policy makers and society. Many efforts are taken at the international level in order to prevent further damages to the environment (e.g. IPCC scientific body since 1988). Yet, many aspects related to our future climate and well-being remains uncertain. For example, melting of polar glaciers and sea-level rise are some of the long-term concerns in climate change projections with uncertain magnitude (Otto-Bliesner et al., 2006a). However, as an old Chinese proverb says "Consider the past and you shall know the future", looking back in past climates can improve our understanding of climate's dynamics and help in addressing key questions for the future (e.g. Past4Future, 2010).

The Earth has experienced quite warm past climates (e.g. interglacials), featured significant reductions in Greenland ice-sheets and considerable sea-level rise. Despite that, analyzing past climate conditions trough geological records is not straightforward since these records are scarce and regionally biased (Kubatzki et al., 2000). Efforts have been made over the last decades to provide more reliable data records. Attention has been particularly paid to the mid-Holocene, the Last Glacial Maximum (LGM) and the Last interglacial (referred here as MIS-5). Because of availability of proxy data, palaeoenvironmental datasets are developed (Braconnot et al., 2004) for (1) the mid-Holocene – BIOME 6000 (Prentice and Webb III, 1998; Prentice et al., 2000) and (2) for the LGM – Tropical terrestrial data synthesis (Farrera et al., 1999). The Palaeoclimate Model Intercomparison project (in its third phase, PMIP3, http://pmip3.lsce.ipsl.fr)has recently extended its focus to include MIS-5 and Pliocene. Up to now there are no detailed datasets compiled for MIS-5 except for the global temperature record of Turney and Jones (2010). This is related to the fact that creating a database based on individual records is complicated (Groll et al., 2005) due to the large uncertainties in estimating the duration of MIS-5 (Shackleton et al., 2003) on one hand and in the climate variability within MIS-5 (Tzedakis et al., 2003) on the other hand.

CPD
8, 5293–5340, 2012

MIS-5 is the last time during which the Arctic experienced noticeable warming, accompanied by sea-level rise and reduction in ice-sheets (Otto-Bliesner et al., 2006a; Kukla et al., 2002; Bintanja et al., 2005; Jouzel et al., 2007; McKay et al., 2011). It offers a suitable candidate for assessing climate models and their response to different forcings. However, MIS-5 climate should not be considered as a full analogue for future climate change because of its different astronomical and greenhouse forcings (Berger and Loutre, 1996; Berger and Yin, 2012). Lunt et al. (same issue) analyze snapshot simulations (which include the simulations used in our present study) between 125 ka and 130 ka BP performed by several climate models. They focus on the analysis of near surface temperature. Here, we present more detailed regional analysis and we consider more variables in the comparison of climate simulations for MIS-5 (127 ka BP) relative to the Pre-Industrial (PI) period, obtained by an Earth system model of intermediate complexity (LOVECLIM) and a comprehensive Atmosphere-Ocean General Circulation Model (CCSM3). This is the first intercomparison between LOVECLIM and CCSM3 models with emphasis on MIS-5 stressing details on the similarities and differences in the simulated large-scale features of surface temperature and their relationships to monsoon, vegetation and ENSO. Whenever possible, the simulation results are compared to proxy data reported in literature, in order to determine where features are robust and where uncertainties are large.

In Sect. 2 we give a brief description of LOVECLIM and CCSM3 models and the prescribed boundary conditions. In Sect. 3 we discuss the similarities and differences in surface temperature between LOVECLIM and CCSM3. In Sect. 4 we elaborate on African, Indian and East Asian monsoons. Vegetation is discussed in Sect. 5 and ENSO variability in Sect. 6. Conclusions are given in Sect. 7.

2 Models description

Yin and Berger (2010, 2012) have simulated the peak climate of the past nine interglacials with LOVECLIM. Using the same boundary conditions, Herold et al. (2012)

CPD
8, 5293–5340, 2012

simulated the climate of the five warmer interglacials of the last 800 ka with CCSM3. The experiments for the last interglacial provided by these studies are analyzed in this paper.

2.1 LOVECLIM

LOVECLIM is a three dimensional Earth system model of intermediate complexity (Goosse et al., 2010). The atmosphere model ECBilt is a quasi-geostrophic model with 3 vertical levels and 5.625° × 5.625° (T21) horizontal resolution (Opsteegh et al., 1998). CLIO is a primitive-equation, free-surface ocean general circulation model coupled to a thermodynamic-dynamic sea ice model (Goosse and Fichefet, 1999). The horizontal resolution is 3° × 3° and there are 20 levels on the vertical in the ocean. VECODE is the vegetation model, developed by Brovkin et al. (1997). Based on annual mean values of several climatic variables, the VECODE model computes the evolution of the vegetation cover described as a fractional distribution of desert, tree and grass in each land grid cell with the same resolution as that of ECBilt. In this study, the atmosphere, ocean-sea ice and vegetation are interactively coupled, and the ice sheets are prescribed as today.

2.2 CCSM3

The Community Climate System Model 3 (CCSM3) is a coupled climate model with components representing the atmosphere, ocean, sea ice and land surface connected by a flux coupler (Collins et al., 2006). The atmospheric model is CAM3 (Collins et al., 2004). CAM3 has 26 vertical levels and a 3.75° × 3.75° horizontal resolution which corresponds to T31 configuration. The land model CLM version 3.0 (Oleson et al., 2004) is integrated on the same horizontal grid as the atmosphere, with each grid box further divided into a hierarchy of land units, soil columns and plant types. The ocean model POP (Smith and Gent, 2002) uses a dipole grid with a horizontal resolution of 3° × 1.5° in longitude and latitude, respectively. Vertically, the model has 25 levels

CPD
8, 5293–5340, 2012

that extend to 4.75 km. The sea-ice model CSIM (Briegleb et al., 2004) is a dynamical model and has the same horizontal resolution as the ocean model POP. Ice sheets are prescribed as today. In the CCSM3 model framework there is no dynamically coupled vegetation module. Instead, vegetation is estimated using the offline vegetation model BIOME4 (Kaplan et al., 2003). CCSM3 output variables (such as temperature, precipitation, cloudiness, etc.) are used to force the BIOME4, to see what would be the vegetation distribution given the simulated climate. BIOME4 has 28 types of plants which can be grouped into 6 major categories – grassland, temperate forest, desert, dry tundra, tundra and boreal forest (Harrison and Prentice, 2003). In addition, tropical and warm-temperate forests are included to illustrate the differences between MIS-5 and PI.

2.3 Boundary conditions

The Pre-Industrial climate has the astronomical configuration of year 1950. The initial parameters like greenhouse gas concentrations and astronomical parameters are given in Table 1 (Yin and Berger, 2010, 2012). The values of eccentricity, obliquity, and longitude of perihelion, calculated by Berger (1978), were used. In our experiments, MIS-5 has the astronomical configuration of 127 ka BP when NH summer occurs at perihelion. MIS-5 climate is driven by much larger eccentricity (0.03937 vs. 0.01672 for PI) and obliquity (24.040° vs. 23.446° for PI). Northern Hemisphere (NH) summer occurring at perihelion, a situation opposite to PI time, leads to much more insolation received on Earth during boreal summer (Fig. 1).

The interglacial simulation is 1000-yr long. The last 100 yr of LOVECLIM and CCSM3 simulations are used for the analysis of surface temperature, monsoon regime, vegetation and ENSO, discussed in Sects. 3, 4, 5 and 6, respectively. The equivalent greenhouse gas (GHG) concentration (contribution of CO_2, CH_4 and N_2O) is taken to be 284 ppmv in MIS-5 and 280 ppmv in PI. As a consequence, the differences observed between MIS-5 and PI climate are mainly driven by the strong astronomically-induced seasonal forcing of MIS-5.

CPD
8, 5293–5340, 2012

3 Surface temperature

MIS-5 is 0.5 °C warmer in LOVECLIM and 0.2 °C cooler in CCSM than their respective PI climate (Table 2). Terrestrial and marine records indicate a warming of about 1.9 °C during MIS-5 relative to preindustrial (Turney and Jones, 2010). LOVECLIM and CCSM3 consequently underestimate the observed warming even when taking into account the uncertainties in these records. Reasons might be due to the lack of interactive ice sheets in both simulations. Cooling is simulated in December-January-February (DJF) and warming in June-July-August (JJA) by both models. LOVECLIM simulates consistently warmer climate than CCSM3. This might be due to the fact that a dynamic vegetation model is included in LOVECLIM but is absent in CCSM3. It is also possibly due to the biases in both models. Goosse et al. (2020) report that in LOVECLIM tropical regions are too warm and the temperature gradient between the Eastern and Western Pacific is underestimated as a consequence of a warmer Eastern Pacific. In CCSM3, Collins et al. (2006) report colder northern (60° N and 90° N) and southern (60° S and 90° S) regions.

3.1 June-July-August surface temperature anomalies

The large continental warming during MIS-5 results from its much higher insolation during boreal summer. Radiative forcing induces a temperature response larger over land than over the ocean due to the large thermal capacity of the ocean. Differences in heat capacity can explain the large variation between land and ocean surface during boreal summer. Both LOVECLIM and CCSM3 show that almost all the continents in JJA are warmer during MIS-5 than during PI, with the largest warming over the Northern Hemisphere (NH) lands (Fig. 2). Intensive warming is simulated in North America and Greenland. Over Canada, the average modeled difference between MIS-5 and PI (referred as anomaly) is +3 °C for CCSM3 and +5 °C for LOVECLIM. Over Greenland, the warming reaches +3 °C and +6 °C respectively in the two models. Warmer boreal summer during the last interglacial has also been simulated by other modeling studies

CPD
8, 5293–5340, 2012

and seen in proxy data. Otto-Bliesner et al. (2006a) modeled more than 4 °C warming with another version of the CCSM model in the northern Hudson Bay–Baffin Island–Labrador Sea region, a 3 °C warming or more over Greenland along the edges of the ice cap and a 2.8 °C in its central part. Warmer Greenland is also reported by Andersen et al. (2004). Duplessy et al. (2007) point out that the summer temperatures were 2–5 °C warmer than today in North Atlantic, Greenland and Arctic. Anderson et al. (2006) reviewed the Arctic climate during the last interglacial based on reconstructed proxy records in terrestrial and marine archives. These reconstructions show that the Arctic summer temperatures were about 4–5 °C warmer than today and associated with a decrease in summer sea ice.

MIS-5 is warmer over Europe as found in other studies (e.g., Kaspar et al., 2005; CAPE, 2006). Large warming occurs over northern Asia, too. The loess records in China show warm and humid conditions during the last interglacial (Porter, 2001; Guan et al., 2007). Both CCSM3 and LOVECLIM simulate over China cooler annual temperatures during MIS-5, but warmer summer, confirming that the strength of the soil development in the loess reflects mostly the summer climatic conditions. Exceptionally, there is a cooling over the monsoonal band of North Africa, which is mainly related to a strengthened African monsoon (see Sect. 4) which increases low level moisture and precipitation. Fischer and Jungclaus (2010) also simulated a temperature decrease in the tropics attributed to the same intensification of the African monsoon system.

Warming is simulated in the Southern Hemisphere (SH) – South Africa, Australia, South America and Antarctica. A reasonable agreement is found between the two model anomalies in Antarctica between 120° W and 0° E at 60° S. A warming of about 2 °C over Antarctica and over the Southern Ocean is detected in proxy records, as shown by Vimeux et al. (2002) and Pahnke et al. (2003), respectively. From marine records and LOVECLIM simulations, Duplessy et al. (2007) conclude that, in the Southern Hemisphere, over the Antarctic Plateau and Southern Ocean, the warming was about 2 °C during the last interglacial period. In the Southern Ocean, CCSM3 shows a dipole anomaly from cooling (−1 °C and −2 °C) to warming (1–4 °C), whereas

CPD
8, 5293–5340, 2012

LOVECLIM shows only warming (from 1–3 °C). These differences near the continental shelves of Antarctica originate from the sea-ice concentration (Figure 3 for CCSM3). CCSM3 simulates more sea-ice, extending further to the North, during MIS-5 than does LOVECLIM. The main drivers for this excessive sea-ice concentration in CCSM3 are reported in several papers (Otto-Bliesner et al., 2006b; Yeager et al., 2006; Gent et al., 2011; Herold et al., 2012) and we will not discuss them further here. In west Antarctic Peninsula, LOVECLIM underestimates the sea-ice extent for reasons explained in Goosse et al. (2010), leading to larger positive temperature differences with PI than in CCSM3.

3.2 December-January-February surface temperature anomalies

During boreal winter both models show cooler continents in MIS-5 than at PI, as a consequence of its reduced insolation (Fig. 4). Cooler MIS-5 is modeled by both models in the tropics of North Africa and the Arabian Peninsula, as well as over East Asia. Over Easther Japan, a negative anomaly between −2.5° and −4 °C is simulated in CCSM3 but not in LOVECLIM. Herold et al. (in press) associate this intensified cooling in CCSM3 with an increased sea-ice formation. Over the oceans, the sea-surface temperature (SST) anomalies are weak in both models (around −0.5 °C), except in the Arctic region and in the Southern Ocean. In the Southern Ocean, LOVECLIM simulates only a warming while CCSM3 simulates a narrow region of warming and large areas of cooling. Crosta et al. (2004) investigated the sea-ice concentration around 55° S at 160° E and found that February SST were between 5–6 °C warmer. Our model simulations show that the warming in this area is consistent with their SST reconstructions. In the area between 52° S and 59° S and 40° E and 35° W, Bianchi and Gersonde (2002) report a warming of 2–3.5 °C which is consistent with our LOVECLIM simulation, but not with CCSM3.

Over most of the Arctic region, the surface temperature anomalies agree pretty well in both models with a smooth south-north transition from cooling to warming. The winter Arctic Ocean sea-surface temperature in MIS-5 remains higher than in PI, a result of

CPD
8, 5293–5340, 2012

the higher summer insolation and its delayed impact in winter though the ocean-sea-ice system, the so-called summer remnant effect (Yin and Berger, 2012). Fischer and Jungclaus (2010) point out that the reduced/absent sea-ice cover over the Barents Shelf and on the east coast of Greenland cannot act as an insulator between the ocean and the atmosphere, confirming the summer remnant effect. The warming is larger in CCSM3 over the Labrador Sea and Davis Strait than in LOVECLIM. This could have a direct effect on the modeled North Atlantic ocean surface temperature as well. A warming over the Davis Strait would increase the melting of the sea ice thus increasing the inflow of fresh, cold water to the Labrador Current. This is, in particular, seen over the North Atlantic Ocean around 45° N and 60° W. CCSM3 simulates a negative surface temperature anomaly in the North Atlantic from −0.5 ° to −2.5 °C which is not seen in the LOVECLIM simulation.

Discrepancy between the two models happens in the Nordic Seas - Svalbard archipelago from 74–81° N and from 10–35° E. CCSM3 simulates a large cooling while LOVECLIM simulates a warming. Bauch et al. (1999) investigated the sea-surface temperature in the area of Iceland, Norwegian and Greenland Seas based on proxy records of planktonic foraminiferal assemblages, $CaCO_3$ content, oxygen isotopes of foraminifera and iceberg-rafted debris. Based on this analysis, it was shown that MIS-5 sea-surface temperature was warmer in comparison with Holocene in Iceland Sea, but remained cooler north of 70° N due to a reduction in the northward flow of Atlantic surface water and less outflow of polar waters from the Arctic Ocean. It was also suggested that a relatively cold northern Eurasian margin could have resulted in more glaciated areas with consequences for the atmospheric circulation patterns, sea-ice cover and albedo. Figure 5a, b shows the anomalies in sea-ice concentration simulated in CCSM3 and LOVECLIM, respectively. LOVECLIM shows negative anomaly of −0.3 %, i.e. less sea-ice concentration south of Svalbard in MIS-5 in comparison with PI. On the contrary, CCSM3 shows a sea-ice expansion with its maximum positive anomaly (+0.4 %) during DJF over the globe. Herold et al. (2012) discuss the possible reasons for such sea-ice formation in CCSM3. Fresh water (due to the melting of sea-ice), entering the

CPD
8, 5293–5340, 2012

Labrador Current from the Davis Strait can contribute to the freshening and cooling of the North Atlantic Current. This would induce two effects: a sea-ice increase at around 45° N and 60° W and a transport of fresh and cold waters to the Nordic Seas resulting in an increased sea-ice formation. Oppo et al. (2001) argue that changes in latitudinal temperature gradients may induce changes in large-scale wind fields with "far-reaching influences". Such influences include, for example, changes in the strength or position of important boundary currents, changes in temperature and salinity in areas of deep water formation, etc. A negative salinity anomaly in CCSM3 is simulated between 10° W and 70° W at around 40° N (not shown). This is not necessarily related to excessive precipitation and dilution, but instead to a fresh water flux from the Davis Strait and Labrador Sea. Also above 80° N, the negative salinity anomaly is significant (up to −2, $-3\,g\,kg^{-1}$) resulting from ice melting during boreal summer and delayed sea-ice formation during boreal winter. LOVECLIM does not simulate such intensive freshening in the North Atlantic Ocean, the anomaly being only between 0 and $0.5\,g\,kg^{-1}$.

So far, such intensified surface temperature negative anomaly during boreal winter of the last interglacial is reported in Herold et al. (2012) and partly shown in Lunt et al. (2012, for CCSM model). Further evaluation is, however, required because such freshening would have a dramatic effect on the Atlantic Meridional Overturning Circulation (Hodell et al., 2009).

3.3 Annual surface temperature

Figure 6 depict the annual differences between MIS-5 and PI simulated by CCSM3 and LOVECLIM, respectively. Warming is simulated in high latitudes by both models. The largest anomalies are towards the North Pole. This warming is a result of the high insolation during summer and the summer remnant effect during winter (Yin and Berger, 2012). On the contrary, over the Southern Ocean, the insolation change during DJF (austral summer) is too small to trigger a summer remnant effect and the annual warming is driven by the global warmth during JJA (austral winter) (Berger and Yin, 2010). Warmer Southern Ocean and an annually warmer Antarctica is modeled in

CPD
8, 5293–5340, 2012

LOVECLIM, but not in CCSM3, except for the area between 60° E and 120° E at around 60° S. There the warming of 0.5–1.5 °C, is in good agreement with the LOVECLIM results (1.5–2 °C). Vostok ice core reveals a 3 °C warming on the Antarctic Plateau (Petit et al., 1999) which was confirmed later by the EPICA ice core showing that Antarctica was 2–4 °C warmer during MIS-5 than PI (Jouzel et al., 2007; Masson-Delmotte et al., 2010).

A good agreement between the two models is found over the continents. Warmer Australia is modeled in LOVECLIM and CCSM3, reflecting the warmth in JJA. Large cooling in the tropics over North Africa and Arabian Peninsula is simulated by both models. This cooling originates from the intense precipitation during JJA and the reduced insolation during DJF. A cooling is also simulated over South Asia (originating from DJF during MIS-5) and over Eastern Japan (related to sea-ice formation). Cooling happens in equatorial Pacific in LOVECLIM, but warm spots are simulated in the NINO3.4 area in CCSM3. Therefore, the ENSO variability simulated by CCSM3 is further investigated in Sect. 6.

Overall, the annual mean response of the two models is small, but the seasonal response is much more clear. This is also discussed by Lunt et al. (2012) in their model intercomparison. They stress that the agreement between models and proxy records is far from perfect and the uncertainties in these proxy records need to be assessed. They also point that MIS-5 climate is modulated by a different astronomical configuration than at PI and this lead to a seasonal shift which could be interpreted as an annual mean change in the proxy data. LOVECLIM simulates higher seasonal and therefore annual mean surface temperatures than CCSM3. Around Svalbard archipelago the strong DJF signal, simulated in CCSM3, is imprinted on the annual surface temperature whereas the JJA signal dominates the LOVECLIM simulations in this region. The uncertainties remain large in the areas of modeled sea-ice formation and need to be further addressed because the majority of the seasonal and annual temperature variations occurs at sea-ice boundaries (Herold et al., 2012).

CPD
8, 5293–5340, 2012

4 Precipitation anomalies

4.1 JJA rainfall

Monsoon is the major manifestation of the seasonal cycle in the tropical regions and there is a wide range of evidence from marine and terrestrial data that the monsoon characteristics are affected by changes in the Earth's astronomical parameters (Noblet et al., 1996; Kubatzki et al., 2000; Montoya et al., 2000) during the last Interglacial. Both CCSM3 and LOVECLIM simulate significantly stronger northern monsoon during MIS-5. As compared to PI (Fig. 7), MIS-5 simulated rainfall increases by 4–5 mm day^{-1} over central Africa and Saudi Arabia and by 3–4 mm day^{-1} over India, Tibet, south-western China and the northern part of South America. These results are in good agreement with the simulated heavy precipitation and proxy data reported in Prell and Kutzbach (1987). The precipitation change is relatively small over the extra-tropical regions.

A strong northward migration and intensification of the Intertropical Convergence Zone (ITCZ) was observed in equatorial Africa with a significant precipitation increase the Sahel and southern Sahara, but less over tropical Africa south of 8° N. The sources of water for our simulated African monsoon are from the tropical Atlantic and from local recycling further inland. The amount of water vapor coming from both sources is enhanced during the last Interglacial due to increased low-level wind speeds and land evaporation rates, as discussed also in Braconnot et al. (2008). Indeed the distribution of precipitation depends very much on the location of moisture sources and on wind speed. The increased low level wind and moisture transport during MIS-5 are in good agreement with heavy tropical boreal summer precipitation in both model simulations.

Over Asia the most prominent shifts in precipitation maxima is related to the northward displacement of the ITCZ. Northward shift of the ITCZ during JJA is seen from the eastern Pacific to India, consistent with a greater increase in JJA insolation in the NH compared to the SH. The increased NH seasonal contrast led to warmer summers and colder winters. Large amounts of water vapor are advected from moisture sources

CPD
8, 5293–5340, 2012

located over the Arabian Sea, the Indian Ocean and west Pacific to Southern Asia. Moreover the northward penetration of moist air is limited by the Tibetan plateau that prevents it from being transported further north. As a consequence Asia experienced stronger summer monsoon in MIS-5. The southern and western branch of the North Pacific high strengthens the East Asian summer monsoon as seen from an increase in onshore winds and in precipitation in northern China for CCSM3 and in most of China in LOVECLIM. The JJA surface wind (Fig. 8) and moisture transport (not shown) during MIS-5 are in good agreement with water vapor supply over East Asia coming mainly from Indian Ocean and secondarily from South China Sea and western Pacific Ocean.

Monsoon rainfall distribution is closely related to large scale atmospheric circulation. The upper level (100 hPa) tropical easterly jet (TEJ) is strong in the simulation in agreement with the heavy rainfall over the tropical monsoon region, because the TEJ is closely linked to the boreal summer monsoon rainfall over Africa and Asia through the Hadley circulation. We found that TEJ was stronger and shifted northward from its mean position during MIS-5 (Fig. 9), consistent with the strong rainfall over the convergence zone between the wind of the southern and northern hemispheres, known as the monsoon trough (Zeng and Guo, 1982). Another extremely important component of the summer monsoon circulation is the upper-level monsoon ridge (in the 200 hPa geopotential height), which normally extends from the Middle East eastward to southeastern Asia. The northward shift of the strong gradient indicates a strong divergence in the upper troposphere which supports the strong monsoon meridional vertical circulation and heavy rainfall over that region. An anomalous high over central Europe, a low over the western Siberia plain and a major high anomaly over northeastern Asia depicts a wave train that has an equivalent barotropic structure in the mid-latitudes. The specific humidity anomaly seen at low level favours also the heavy rain simulated over Africa, India and East Asia. The JJA meridional average (Equator to 40° N) vertical velocity indicates more convection and heavier rainfall especially over the African and Asian domains (Fig. 10). Our 100-yr simulated Indian monsoon index (IMI) for JJA (Wang and Fan, 1999) shows that IMI is definitely stronger during MIS-5 (Fig. 11).

CPD
8, 5293–5340, 2012

There is more precipitation during MIS-5 in LOVECLIM than in CCSM3 (Table 3, JJA). A major precipitation difference between two models is found over tropical Indian Ocean, tropical central Pacific Ocean, tropical Atlantic Ocean, North America and East Asia. For example over East Asia, in LOVECLIM, summer precipitation increases over southern and eastern China and over Japan during MIS-5 when compared to PI. But in CCSM3, it decreases over eastern China and Japan. This could be a bias of CCSM3 because, in particular, stalagmite from eastern China (Wang et al., 2008) and lake sediments from Japan (Xiao et al., 1999) indicate stronger summer monsoon precipitation during MIS-5 than today.

4.2 DJF rainfall

In DJF, both CCSM3 and LOVECLIM simulate more rain during MIS-5 over the Indian Ocean, west Pacific, north east and south east Pacific, but less over the subtropical southern continents (South America, central Africa, and Australia). The weakening of the southern summer monsoon during MIS-5 is in agreement with the modeling results of Montoya et al. (2000) and with some proxy records. For example, Tofalo et al. (2011) from their analysis of loess-paleosols records in Argentina conclude to a drier MIS-5 climate. High pollen concentrations and high percentage of henopodiaceae/Amaranthaceae from the lake Titicaca (Bolivia-Peru) indicate warmth and aridity during MIS-5 (Fritz et al., 2007). Zhao et al. (2001) shows that the stalagmite growth in Western Australia during MIS-5 was slow implying dry conditions. Ayliffe et al. (1998) discuss that during interglacials and warm interstadials the southeastern part of Australia was comparatively arid. In general, the estimate of precipitation is more difficult than temperature and reconstructions of past precipitation are less common and quantitative. Hence, there is a need of additional data from the Southern Hemisphere (especially over land) that could increase our understanding of the past climate conditions and provide the necessary data for model evaluation.

CPD
8, 5293–5340, 2012

5 Vegetation

Figure 12a–c and Fig. 13 show the vegetation simulated in MIS-5 and PI for LOVECLIM and CCSM3-BIOME4, respectively. Similarities are observed in the modeled vegetation during MIS-5 between LOVECLIM and CCSM3-BIOME4. LOVECLIM shows a higher percentage of tree fraction between the Equator and 30° N in MIS-5 than CCSM3-BIOME4 in the tropical forest. Braconnot et al. (2007) highlighted (although for Mid-Holocene) that precipitation in their model intercomparison is severely underestimated and not sufficient to sustain grass (steppe) in place of desert, except for LOVECLIM. This could be related to biases in LOVECLIM, i.e. overestimation of precipitation around 30° N and temperature in the tropics (Goosse et al., 2010). Biases in precipitation can cause unrealistic distribution of plant types that can amplify the vegetation feedback response. However, the expansion of the vegetated area resulting from the African summer monsoon, simulated in LOVECLIM, is in line with proxy records, showing wetter, more green and vegetated Sahel/Sahara (Jolly et al., 1998). Tropical forest and grassland are abundant as a result of the northward shift of the inter-tropical convergence zone and moisture advection. Grassland simulated in CCSM3-BIOME4 occupies about 70 % of the land at 20° N while LOVECLIM simulates about 50 % and the rest is mainly trees.

Mid-latitude grass simulated in CCSM3-BIOME4 is more abundant than in LOVECLIM over Europe, Asia and central North America (between 30° N and 60° N). The temperate forest simulated in CCSM3-BIOME4 decreases significantly when compared to its PI level. The abundance of grass and decrease of forest simulated in CCSM3-BIOME4 could be associated with colder annual climate and negative precipitation anomaly in CCSM3 that could affect the distribution of vegetation. According to Brovkin (2002), climate exerts a major control on the spatial distribution of vegetation types while vegetation influences climate via changes in the physical properties of the land surface such as albedo, biogeophysical mechanisms, roughness and atmospheric gas composition. Denman et al. (2007, IPCC report Climate Change 2007) claim that

CPD
8, 5293–5340, 2012

"Shorter vegetation with more leaves has the most latent heat flux and the least sensible flux. Replacement of forests with shorter vegetation together with the normally assumed higher albedo could then cool the surface". Vegetation induced cooling through albedo change is discussed in several studies (Ganopolski et al., 1998; Claussen, 1998; Claussen et al., 2006; Kubatzki et al., 2000). LOVECLIM simulates warmer annual climate and positive precipitation anomaly with higher tree fraction below 45° N and similar between 45° N and 60° N to its PI level. Proxy data reveal that mixed forest is well established in Europe (Kukla et al., 2002; Muller et al., 2003). For Shackleton et al. (2003), MIS-5 is a time with decrease in steppe and increase in forest elements; it means a rise in Eurosiberian and Mediterranean trees. During MIS-5, the vegetation in the Chinese loess plateau which is particularly sensitive to climate warming is a mixture of steppe and forest (Cai et al., 2012).

Wetter and warmer climate in high northern latitudes (between 60° N and 70° N) promote the growth and shift to the north of boreal forest, seen in both modeled results. Tundra and boreal forest in CCSM3-BIOME4 and trees and grass in LOVECLIM simulations are found in good agreement. CAPE group members (2006) report fossil pollen data and proxy evidence that the boreal forests experienced "dramatic poleward expansions". Tundra, grass and forest (proxy data indicate mainly birch forest) flourished on the western and eastern sides of Greenland. Notable northward shift of boreal forest across the Arctic is also reported in Saarnisto et al. (1999) for Scandinavia, in Lozhkin et al. (2007) for Siberia and in Edwards et al. (2003) for Alaska.

A large reduction in desert, as compared to PI, is simulated in both models over the Northern Hemisphere (Fig. 12c for LOVECLIM and Fig. 13 panel desert for CCSM3-BIOME4). Over the Southern Hemisphere, CCSM3-BIOME4 and LOVECLIM simulations are found in a good agreement. The increase in desert between the Equator and 30° S is attributed to the annual warming and decreased precipitation over Australia.

CPD
8, 5293–5340, 2012

6 Mean climate and variability of the tropical pacific

In this section we discuss the warm spots seen in the equatorial Pacific partly mentioned in Sect. 3. The annual cycles of equatorial tropical Pacific sea surface temperature (SST), zonal wind stress and mean tilt of the thermocline are averaged over 5° S–5° N and analyzed. In the CCSM3 simulations, MIS-5 SST field shows a westward shift in the Pacific cold tongue (minimum SST), an eastward shift of the warm pool (maximum SST) and a cooling mainly in the central Pacific relative to the PI (Fig. 14a). The east-west SST difference (difference between cold tongue and warm pool) increases slightly from 4 °C in PI to 4.2 °C in MIS5. This is not the case for LOVECLIM which shows only an east-west SST difference of 2 °C due to its biases in SST (Goosse et al., 2010) that would cause smaller ENSO variability. For CCSM3, the zonal wind stress shows a very slight decrease mainly in the eastern and western sides in MIS-5 (Fig. 14b). In LOVECLIM, however, there is a significant increase in the MIS-5 zonal wind stress when compared to PI. This wind stress has an effect on the depth of the thermocline which is approximated by the depth of the 20 °C-isotherm as is usually done by model studies of PI and as assumed here for MIS-5. In CCSM3, there is almost no difference in the thermocline between MIS-5 and PI (Fig. 14c) which is consistent with the very small difference in the zonal wind stress. In contrast, LOVECLIM shows a much deeper thermocline for MIS-5 especially in the western part. Based on the finding of Timmermann et al. (2005), we suggest that this deepening of the thermocline is an ocean-related process most likely caused by its re-adjustment to the weakening of the Atlantic meridional circulation (AMOC). The fact that we found the thermocline deepening only in our LOVECLIM simulation might be related to its lower atmosphere resolution. Indeed, in response to AMOC weakening, more complex models also exhibit a change in their atmospheric circulation which in turn can cause a shoaling of the thermocline and restrains the thermocline from deepening through the oceanic processes (Timmermann et al., 2007a).

CPD
8, 5293–5340, 2012

For the ENSO variability around the mean state, the last 1200 months of SSTs were used. We focused on the so-called NINO3.4 region (5° S–5° N; 190–240° E) and averaged SST over this region. The monthly mean cycle was resolved, and a 12-month moving average filter was applied following Douglass (2011). We find the NINO3.4 SST variability in our LOVECLIM simulations to be particularly small as it might have been expected from their overestimated deep thermocline which diminishes the SST variability. We will, therefore, mainly discuss the ENSO characteristics of the CCSM experiments.

Figure 15a shows the spectrum of the SST NINO3.4 anomalies. The dominant period of ENSO variability (highest peak of the spectra) in PI experiment is around 3.7 yr, next to two other smaller peaks with periods of around 5 and 1.7 yr. We also find a period of around 2–3 yr when we use another spectral technique or apply a 5-month moving average filter (the 3.7-yr period becoming then a secondary peak). This is more or less consistent with some other CCSM3 model studies where a period of around 2 yr for ENSO variability was found (e.g., Merkel et al., 2010). In the MIS-5 run, the leading period is around 2.1 yr, and its amplitude is slightly larger than in the PI case. This apparently shorter period for MIS-5-simulated ENSO might be partially related to the westward shift of the cold tongue that reduces the distance and consequently the travel time for the Rossby waves between the cold tongue and the warm pool. A stronger amplitude of ENSO in MIS-5 can in some degree be related to the shoaling of the thermocline, the increase of the east-west temperature gradient and the weaker trade winds in the tropical Pacific. However, as was shown above, the change in these factors was not significant and other factors should be considered. If a stronger ENSO is found in MIS-5 relatively to PI, we suggest, following Timmermann et al. (2007b), that the change in the strength of the SST annual cycle of MIS-5 could be the main cause to enhance the ENSO strength. Figure 15c shows that, during MIS-5, the SST are larger than during PI from March to November. At the same time, the variance for each individual month is smaller during MIS-5 than at PI (Fig. 15b). Although this variance

CPD
8, 5293–5340, 2012

is not necessarily reflecting only ENSO activity, it remains that, for each month, there seems to be a negative correlation between the mean value and the variability of SST.

7 Conclusions

In this paper we presented a comparison of modeled results from LOVECLIM and CCSM3 simulations between MIS-5 and PI climates for surface temperature, hydrological cycle, vegetation and ENSO. We described the similarities and differences in the modeled features between the two models, and compared modeled results with proxy data reported in literature.

Overall, LOVECLIM simulates higher annual and seasonal mean surface temperatures than CCSM3. Arctic remains warmer through the whole year because of high insolation and summer remnant effect and Antarctica is annually warmer due to the global warmth during JJA. CCSM3 simulates larger tropical Pacific SST for MIS-5 and a tendency for El Nino type of climate. The dominant period of ENSO is found to change from 3.7 yr in the PI experiment to 2.1 yr in MIS-5, that we suggest is related to the change in the SST annual cycle next to smaller effects through increased east-west temperature gradient and less-steep thermocline. Continents remain warmer during summer (except over North Africa and Arabian Peninsula) and cooler during winter in MIS-5. The cooling during boreal summer over North Africa and Arabian Peninsula is caused by increased precipitation due to intensified African monsoon. In Africa, during JJA, the rain band expands further north while over India maxima precipitation is pushed further west. Precipitation increases over the Sahel and southern Sahara, over India, Tibet, southwestern China and over the northern part of South America. Vegetation (grassland and forest) increases over Sahel/Sahara due to sufficient moisture supply. Mid-latitude forest decreases in BIOME4 but remains near its PI level in LOVECLIM. Tundra and boreal forest expand deep in high northern latitudes. Large reduction in desert land is simulated in the Northern Hemisphere, whereas increase in desert is simulated in North Australia due to the annual warming and decreased precipitation.

CPD
8, 5293–5340, 2012

The Earth's climate for the last interglacial remains not fully resolved because from one hand data are scarce and mostly confined to the Northern Hemisphere and from the other hand the interpretations are regional biased (Kubatzki et al., 2000). Hence, there is a need of additional data from the tropics and Southern Hemisphere that could increase not only our understanding of the past climate dynamics, but can provide the so necessary data for model assessment because comparisons between model simulations and proxy data is a key to test the credibility of the proposed methods.

Acknowledgements. This work and I. Nikolova, U. K. Singh and M. P. Karami are supported by the European Research Council Advanced Grant EMIS (No 227348 of the Program "Ideas"). Q. Z. Yin is supported by the Belgian National Fund for Scientific Research (F. R. S.-FNRS). N. Herold is thanked for the simulations with CCSM3. Access to computer facilities was made easier through sponsorship from S. A. Electrabel, Belgium.

References

An, Z. S., Liu, T. S., Lu, Y. C., Porter, S. C., Kukla, G., Wu, X. H., and Hua, Y.: The long- term paleomonsoon variation recorded by the loess-paleosol sequence in central China, Quatern. Int., 7, 91–96, 1990.

Andersen, K. K., Azuma, N., Barnola, J.-M., Bigler, M., Biscaye, P., Caillon, N., Chappellaz, J., Clausen, H. B., Dahl-Jensen, D., Fischer, H., Flückiger, J., Fritzsche, D., Fujii, Y., Goto- Azuma, K., Grønvold, K., Gundestrup, N. S., Hansson, M., Huber, C., Hvidberg, C. S., Johnsen, S. J., Jonsell, U., Jouzel, J., Kipfstuhl, S., Landais, A., Leuenberger, M., Lorrain, R., Masson-Delmotte, V., Miller, H., Motoyama, H., Narita, H., Popp, T., Rasmussen, S. O., Raynaud, D., Rothlisberger, R., Ruth, U., Samyn, D., Schwander, J., Shoji, H., Siggard-Andersen, M.-L., Steffensen, J. P. S., T., Sveinbjörnsdóttir, A. E., Svensson, A., Takata, M., Tison, J.-L., Thorsteinsson, T., Watanabe, O., Wilhelms, F., and White, J. W. C.: High-resolution record of Northern Hemisphere climate extending into the last interglacial period, Nature, 431, 147–151, 2004.

Anderson, P., Bermike, O., Bigelow, N., Brigham-Grette, J., Duvall, M., Edwards, M. E., Frechette, B., Funder, S., Johnsen, S., Knies, J., Koerner, R., Lozhkin, A., Marshall, S., Matthiessen, J., Macdonald, G., Miller, G., Montoya, M., Muhs, D., Otto-Bliesner, B., Over-

CPD
8, 5293–5340, 2012

peck, J., Reeh, N., Sejrup, H., Spielhagen, R., Turner, C., and Velichko, A.: Last Interglacial Arctic warmth confirms polar amplification of climate change, Quatern. Sci. Rev., 25, 1383–1400, doi:10.1016/j.quascirev.2006.01.033, 2006.

Ayliffe, L. K., Marianelli, P. C., Moriarty, K. C., Wells, R. T., McCulloch, M. T., Mortimer, G. E., and Hellstrom, J. C.: 500 ka precipitation record from southeastern Australia: evidence for interglacial relative aridity, Geology, 26, 147–150, 1998.

Bauch, H. A., Erlenkeuser, H., Fahl, K., Spielhagen, R. F., Weinelt, M. S., Andruleit, H., and Henrich, R.: Evidence for a steeper MIS5 than Holocene sea surface temperature gradient between Arctic and sub-Arctic regions, Palaeogeogr. Palaeocl., 145, 95–117, 1999.

Berger, A.: Long Term Variations of Daily Insolation and Quaternary Climatic Changes, J. Atmos. Sci., 35, 2362–2367, 1978.

Berger, A. and Loutre, M.-F.: Modélisation de la réponse du climat au forçage astronomique et à la concentration en CO_2. Comptes rendus de l'Académie des sciences. Série 2, Sciences de la terre et des planètes, 323, 1–16, 1996.

Berger, A. and Yin, Q. Z.: Modelling the past and future interglacials in response to astronomical and greenhouse gas forcing, The Future of the World's Climate, Elsevier, Amsterdam, ISBN: 9780123869173, 437–462, 2012.

Bianchi, S. and Gersonde, R.: The Southern Ocean surface between Marine Isotope Stages 6 and 5d: shape and timing of climate changes, Palaeogeogr. Palaeocl., 187, 151–177, 2002.

Bintanja, R., van de Wal, R. S. W, and Oerlemans, J.: Modelled atmospheric temperatures and global sea levels over the past million years, Nature, 437, 125–128, 2005.

Braconnot, P., Harrison, S. P., Joussaume, S., Hewitt, C. D., Kitoch, A., Kutzbach, J. E., Liu, Z., Otto-Bliesner, B., Syktus, J., and Weber, S. L.: Evaluation of PMIP coupled ocean-atmosphere simulations of the mid-Holocene, Dev. Paleoenviron. Res., 6, 515–533, 2004.

Braconnot, P., Otto-Bliesner, B., Harrison, S., Joussaume, S., Peterchmitt, J.-Y., Abe-Ouchi, A., Crucifix, M., Driesschaert, E., Fichefet, Th., Hewitt, C. D., Kageyama, M., Kitoh, A., Laîné, A., Loutre, M.-F., Marti, O., Merkel, U., Ramstein, G., Valdes, P., Weber, S. L., Yu, Y., and Zhao, Y.: Results of PMIP2 coupled simulations of the Mid-Holocene and Last Glacial Maximum – Part 1: experiments and large-scale features, Clim. Past, 3, 261–277, doi:10.5194/cp-3-261-2007, 2007.

Braconnot, P., Marzin, C., Grégoire, L., Mosquet, E., and Marti, O.: Monsoon response to changes in Earth's orbital parameters: comparisons between simulations of the Eemian and of the Holocene, Clim. Past, 4, 281–294, doi:10.5194/cp-4-281-2008, 2008.

CPD
8, 5293–5340, 2012

Briegleb, B. P., Bitz, C. M., Hunke, E. C., Lipscomb, W. H., Holland, M. M., Schramm, J. L., and Moritz, R. E.: Scientific description of the sea ice component in the Community Climate System Model, Version Three. Technical Report NCAR/TN-463+STR, National Center for Atmospheric Research, Boulder, CO, 80307–3000, 2004.

Brovkin, V.: Climate-vegetation interaction, J. Phys IV France, 12, 57–52, doi:10.1051/jp4:20020452, 2002.

Brovkin, V., Ganopolski, A., and Svirezhev, Y. : A continuous climate-vegetation classification for use in climate-biosphere studies, Ecol. Model., 101, 251–261, 1997.

Cai, M., Wei, M., Fang, X., Xu, D., Miao, Y., and Wu, F.: Vegetation and climate change during three interglacial periods represented in the Luochuan loess-paleosol section, on the Chinese Loess Plateau, Quartern. Int., doi:10.1016/j.quaint.2012.06.041, in press, 2012.

Caillon, N., Severinghaus, J. P., Barnola, J.-M., Chappellaz, J., Jouzel, J., and Parrenin, F.: Estimation of temperature change and of gas age-ice age difference, 108 kyr BP, at Vostok, Antarctica, J. Geophys. Res., 106, 31893–31901, 2001.

CAPE-Last Interglacial Project Members: Last interglacial Arctic warmth confirms polar amplification of climate change, Quaternary Sci. Rev., 25, 1383–1400, 2006.

Claussen, M.: On multiple solutions of the atmosphere-vegetation system in present-day climate, Glob. Change Biol., 4, 549–559, 1998.

Claussen, M., Fohlmeister, J., Ganopolski, A., and Brovkin, V.: Vegetation dynamics amplifies precessional forcing, Geophys. Res. Lett., 33, L09709, doi:10.1029/2006GL026111, 2006.

Collins, W. D., Rasch, P. J., Boville, B. A., Hack, J. J., McCaa, J. R., Williamson, D. L., Kiehl, J. T., Briegleb, B., Bitz, C., Lin, S.-J., Zhang, M., and Dai, Y.: Description of the NCAR Community Atmosphere Model (CAM3), Technical Report NCAR/TN-464+STR, National Center for Atmospheric Research, Boulder, Colorado 80307–3000, 226, 2004.

Collins, W., Bitz, C. M., Blackmon, M. L., Bonan, G. B., Bretherton, C. S., Carton, J. A., Chang, P., Doney, S. C., Hack, J. J., Henderson, T. B., Kiehl, J. T., Large, W. G., McKenna, D. S., Santer, B. D., and Smith, R. D.: The Community Climate System Model Version 3 (CCSM3), J. Climate, 19, 2122–2143, 2006.

Crosta, X., Sturm, A., Armand, L., and Pichon, J.-J.: Late Quaternary sea ice history in the Indian sector of the Southern Ocean as recorded by diatom assemblages, Mar. Micropaleontol., 50, 209–223, 2004.

Gent, P. R., Danabasoglu, G., Donner, L. J., Holland, M. M., Hunke, E. C., Jayne, S. R., Lawrence, D. M., Neale, R. B., Rasch, J., Vertenstein, M., Worley, P. H., Yang, Z. L., and

CPD
8, 5293–5340, 2012

Zhang, M.: The community climate system model version 4, J. Climate, 24, 4973–4991, 2011.
Denman, K. L., Brasseur, G., Chidthaisong, A., Ciais, P., Cox, P. M., Dickinson, R. E., Hauglustaine, D., Heinze, C., Holland, E., Jacob, D., Lohmann, U., Ramachandran, S., da Silva Dias, P. L., Wofsy, S. C., and Zhang, X.: Couplings Between Changes in the Climate System and Biogeochemistry, in: Climate Change 2007: The Physical Science Basis. Contribution of Working Group I to the Fourth Assessment Report of the Intergovernmental Panel on Climate Change, edited by: Solomon, S., Qin, D., Manning, M., Chen, Z., Marquis, M., Averyt, K. B., Tignor, M., and Miller, H. L., Cambridge University Press, Cambridge, United Kingdom and New York, NY, USA, 1009 pp., ISBN: 9780521705967, 2007.
Ding, Y. and Chan, J. C. L.: The East Asian summer monsoon: an overview, Meteorol. Atmos. Phys., 89, 117–142, 2005.
Douglas, D. H.: Separation of a signal of interest from a seasonal effect in geophysical data: El Niño/La Niña phenomenon, Intern. J. Geosci., 2, 414–419, doi:10.4236/ijg.2011.24045, 2011.
Duplessy, J. C., Roche, D. M.. and Kageyama, M.: The deep ocean during the last interglacial period, Science, 316, 971–975, doi:10.1126/science.1138582, 2007.
Edwards, M. E., Hamilton, T. D., Elias, S. A., Bigelow, N. H., and Krumhardt, A. P.: Interglacial extension of the boreal forest limit in the Noatak valley, northwest Alaska: evidence from an exhumed river-cut bluff and debris apron. Arct, Antarct. Alp. Res., 35, 460–468, 2003.
Farrera, I., Harrison, S. P., Prentice, I. C., Ramstein, G., Guiot, J., Bartlein, P. J., Bonnefille, R., Bush, M., Cramer, W., von Grafenstein, U., Holmgren, K., Hooghiemstra, H., Hope, G., Jolly, D., Lauritzen, S.-E., Ono, Y., Pinot, S., Stute, M., and Yu, G.: Tropical climates at the last glacial maximum: a new synthesis of terrestrial palaeoclimate data. I. Vegetation, lake-levels and geochemistry, Clim. Dynam., 15, 823–856, 1999.
Fischer, N. and Jungclaus, J. H.: Effects of orbital forcing on atmosphere and ocean heat transports in Holocene and Eemian climate simulations with a comprehensive Earth system model, Clim. Past, 6, 155–168, doi:10.5194/cp-6-155-2010, 2010.
Fritz, S. C., Baker, P. A., Seltzer, G. O., Ballantyne, A., Tapia, P., Cheng, H., and Edwards, R. L.: Quaternary glaciation and hydrologic variation in the South American tropics as recontructed from the Lake Titicaca drilling project, Quaternary Res., 68, 410–420, 2007.

CPD
8, 5293–5340, 2012

Ganopolski, A., Kubatzki, C., Claussen, M., Brovkin, V., and Petoukhov, V.: The influence of vegetation-atmosphere-ocean interaction on climate during the Mid-Holocene, Science, 280, 1916–1919, 1998.

Goosse, H. and Fichefet, T.: Importance of ice-ocean interactions for the global ocean circulation: a model study, J. Geophys. Res., 104, 23337–23355, 1999.

Goosse, H., Brovkin, V., Fichefet, T., Haarsma, R., Huybrechts, P., Jongma, J., Mouchet, A., Selten, F., Barriat, P.-Y., Campin, J.-M., Deleersnijder, E., Driesschaert, E., Goelzer, H., Janssens, I., Loutre, M.-F., Morales Maqueda, M. A., Opsteegh, T., Mathieu, P.-P., Munhoven, G., Pettersson, E. J., Renssen, H., Roche, D. M., Schaeffer, M., Tartinville, B., Timmermann, A., and Weber, S. L.: Description of the Earth system model of intermediate complexity LOVECLIM version 1.2, Geosci. Model Dev., 3, 603–633, doi:10.5194/gmd-3-603-2010, 2010.

Groll, N., Widmann, M., Jones, J. M., Kaspar, F., and Lorenz, S. J.: Simulated relationships between regional temperatures and large-scale circulation: 125 kyr BP (MIS5) and the preindustrial period, J. Climate, 18, 4032–4055, 2005.

Guan, Q. Y., Pan, B. T., Gao, H. S., Li, B. Y., Wang J. P., and Su, H.: Instability characteristics of the East Asian Monsoon recorded by high resolution loess sections from the last interglacial (MIS5), Sci. China Ser. D, 50, 1067–1075, 2007.

Harrison, S. P. and Prentice, C. I.: Climate and CO_2 controls on global vegetation distribution at the last glacial maximum: Analysis based on palaeovegetation data, biome modelling and palaeoclimate simulations, Glob. Change Biol., 9, 983–1004, 2003.

Herold, N., Yin, Q. Z., Karami, M. P., and Berger, A.: Modelling the climatic diversity of the warm interglacials, Quaternary Sci. Rev., 56, 126–141, doi:10.1016/j.quascirev.2012.08.020, 2012.

Hodell, D. A., Minth, E. K., Curtis, J. H., McCave, I. N., Hall, I. R., Channell, J. E. T., and Xuan, C.: Surface and deep-water hydrography on Gardar Drift (Iceland Basin) during the last interglacial period, Earth Planet. Sc. Lett., 288, 10–19, 2009.

Jolly, D., Prentice, I. C., Bonnefille, R., Ballouche, A., Bengo, M., Brenac, P., Buchet, G., Burney, D., Cazet, J.-P., Cheddadi, R., Edorh, T., Elenga, H., Elmoutaki, S., Guiot, J., Laarif, F., Lamb, H., Lezine, A.-M., Maley, J., Mbenza, M., Peyron, O., Reille, M., Reynaud-Farrera, I., Riollet, G., Ritchie, J. C., Roche, E., Scott, L., Ssemmanda, I., Straka, H., Umer, M., Van Campo, E., Vilimumbalo, S., Vincens, A., and Waller, M.: Biome reconstruction from pollen and plant

CPD
8, 5293–5340, 2012

macrofossil data for Africa and the Arabian peninsula at 0 and 6000 years, J. Biogeogr., 25, 1007–1027, 1998.

Jouzel, J., Masson-Delmotte, V., Cattani, O., Dreyfus, G., Falourd, S., Hoffmann, G., Minster, B., Nouet, J., Barnola, J. M., Chappellaz, J., Fischer, H., Gallet, J. C., Johnsen, S., Leuenberger, M., Loulergue, L., Luethi, D., Oerter, H., Parrenin, F., Raisbeck, G., Raynaud, D., Schilt, A., Schwander, J., Selmo, E., Souchez, R., Spahni, R., Stauffer, B., Steffensen, J. P., Stenni, B., Stocker, T. F., Tison, J. L., Werner, M., and Wolff, E. W.: Orbital and Millennial Antarctic Climate Variability over the Past 800,000 Years, Science, 317, 793–797, 2007.

Kageyama, M., Peyron, O., Pinot, S., Tarasov, P., Guiot, J., Joussaume, S., and Ramstein, G.: The Last Glacial Maximum climate over Europe and western Siberia: a PMIP comparison between models and data, Clim. Dynam., 17, 23–43, 2007.

Kaplan, J. O., Bigelow, N. H., Prentice, I. C., Harrison, S. P., Bartlein, P. J., Christensen, T. R., Cramer, W., Matveyeva, N. V., McGuire, A. D., Murray, D. F., Razzhivin, V. Y., Smith, B., Walker, D. A., Anderson, P. M., Andreev, A. A., Brubaker, L. B., Edwards, M. E., and Lozhkin, A. V.: Climate change and arctic ecosystems II: Modeling, paleodata-model comparisons, and future projections, J. Geophys. Res., 108, 8171, doi:10.1029/2002JD002559, 2003.

Kaspar, F., Kuhl, N., Cubasch, U., and Litt, T.: A model-data comparison of European temperatures in the MIS5 interglacial, Geophys. Res. Lett., 32, L11703, doi:10.1029/2005GL022456, 2005.

Kubatzki, C., Montoya, M., Rahmstorf, S., Ganopolski, A., and Claussen, M.: Comparison of the last interglacial climate simulated by a coupled global model of intermediate complexity and an AOGCM, Clim. Dynam., 16, 799–814, 2000.

Kukla, G. J., Bender, M. L., de Beaulieu, J. L., Bond, G., Broecker, W. S., Cleveringa, P., Gavin, J. E., Herbert, T. D., Imbrie, J., Jouzel, J., Keigwin, L. D., Knudsen, K. L., McManus, J. F., Merkt, J., Muhs, D. R., Muller, H., Poore, R. Z., Porter, S. C., Seret, G., Shackleton, N. J., Turner, C, Tzedakis, P. C., and Winograd, I. J.: Last Interglacial Climates, SGS Staff-Published Research, Paper 174, http://digitalcommons.unl.edu/usgsstaffpub/174, 2002.

Landais, A., Chappellaz, J., Delmotte, M., Jouzel, J., Blunier, T., Bourg, C., Caillon, N., Cherrier, S., Malaize, B., Masson-Delmotte, V., Raynaud, D., Schwander, J., and Steffensen, J. P.: A tentative reconstruction of the last interglacial and glacial inception in Greenland based on new gas measurements in the Greenland Ice Core Project (GRIP) ice core, J. Geophys. Res., 108, 4563, doi:10.1029/2002JD003147, 2003.

CPD
8, 5293–5340, 2012

Lozhkin, A. V., Anderson, P. M., Matrosova, T. V., and Minyuk, P. S.: The pollen record from El'gygytgyn Lake: implications for vegetation and climate histories of northern Chukotka since the late middle Pleistocene, J. Paleolimnol., 37, 135–153, 2007.

Masson-Delmotte, V., Stenni, B., Pol, K., Braconnot, P., Cattani, O., Falourd, S., Kageyama, M., Jouzel, J., Landais, A., Minster, B., Barnola, J. M., Chappellaz, J., Krinner, G., Johnsen, S., Röthlisberger, R., Hansen, J., Mikolajewicz, U., and Otto-Bliesner, B.: EPICA Dome C record of glacial and integlacial intensities, Quaternary Sci. Rev., 29, 113–128, 2010.

McKay, N. P., Overpeck, J. T., and Otto-Bliesner, B. L: The role of ocean therma; expansion in last interglacial sea level rise, Geophys. Res. Lett., 38, L14605, doi:10.1029/2011GL048280, 2011.

Merkel, U., Prange, M., and Schulz, M.: ENSO variability and teleconnestions during glacial climates, Quaternary Sci. Rev., 29, 86–100, 2010.

Montoya, M., von Storch, H., and Crowley, T. J.: Climate simulation for 125 kyr BP with a coupled ocean-atmosphere general circulation model, J. Climate, 13, 1057–1072, 2000.

Noblet, N. de, Braconnot, P., Joussaume S., and Masson, V.: Sensitivity of simulated Asian and African summer monsoons to orbitally induced variations in insolation 126, 115 and 6 kBP, Clim. Dynam., 12, 589–603, 1996.

Oleson, K. W., Dai, Y., Bonan, G. B., Bosilovich, M., Dickinson, R., Dirmeyer, P., Hoffman, F., Houser, P., Levis, S., Niu, G.-Y., Thornton, P., Vertenstein, M., Yang, Z.-L., and Zeng, X. : Technical description of the Community Land Model (CLM), Technical Report NCAR/TN-461+STR, National Center for Atmospheric Research, Boulder, CO, 80307-3000, 174, 2004.

Oppo, D. W., Keigwin, L. D., and McManus, J. F.: Persistent subtropical climate variability in marine isotope stage 5 and Termination II, Paleoceanography, 16, 280–292, 2001.

Opsteegh, J. D., Haarsma, R. J., Selten, F. M., and Kattenberg, A.: ECBILT: A dynamic alternative to mixed boundary conditions in ocean models, Tellus, 50A, 348–367, 1998.

Otto-Bliesner, B., Marshall, S. J., Miller, G. H., Hu, A., and CAPE Last Interglacial Project members: Simulating Arctic climate warmth and icefield retreat in the last interglaciation, Science, 311, 1751–1753, doi:10.1126/science.1120808, 2006a.

Otto-Bliesner, B. L., Tomas, R., Brady, E. C., Ammann, C., Kothavala, Z., and Clauzet, G.: Climate sensitivity of moderate- and low-resolution versions of CCSM3 to preindustrial forcings, J. Climate, 19, 2567–2583, 2006b.

Pahnke, K., Zahn, R., Elderfield, H., and Schulz, M.: 340 000-year centennial scale marine record of Southern Hemisphere climatic oscillation, Science, 301, 948–952, 2003.

CPD
8, 5293–5340, 2012

Past4Future project: http://www.past4future.eu/index.php/about/about-past4future, 2010.
Petit, J. R. , Jouzel, J., Raynaud, D., Barkov, N. I., Barnola, J.-M., Basile, I., Benders, M., Chappellaz, J., Davis, M., Delaygue, G., Delmotte, M., Kotlyakov, V. M., Legrand, M., Lipenkov, V. Y., Lorius, C., Pépin, L., Ritz, C., Saltzmann, E., and Stievenard, M.: Climate and atmospheric history of the past 420 000 years from Vostok ice core, Antarctica, Nature, 399, 429–436, 1999.
Porter, S. C.: Chinese loess record of monsoon climate during the last glacial-interglacial cycle, Earth-Sci. Rev., 54, 115–128, 2001.
Prell, W. L. and Kutzbach, J. E.: Monsoon Variability over the Past 150 000 Years, J. Geophys. Res., 92, 8411–8425, 1987.
Prentice, I. C. and Webb III, T.: BIOME 6000: reconstructing global mid-Holocene vegetation patterns from palaeoecological records, J. Biogeogr., 25, 997–1005, 1998.
Prentice, I. C., Jolly, D., and BIOME 6000 participants: Mid-Holocene and glacial-maximum vegetation geography of the northern continents and Africa, J. Biogeogr., 27, 507–519, 2000.
Saarnisto, M., Eriksson, B., and Hirvas, H.: Tepsankumpu revisited- pollen evidence of stable MIS5 climates in Finnish Lapland, Boreas, 28, 12–22, 1999.
Shackleton, N. J., Sanchez-Goni, M. F., Pailler, D., and Lancelot, Y.: Marine isotope substage 5e and the MIS5 interglacial, Global Planet, Change, 36, 151–155, doi:10.1016/S0921-8181(02)00181-9, 2003.
Shi, Z., Liu, X. and Cheng, X.: Anti-phased response of northern and southern East Asian summer precipitation to ENSO modulation of orbital forcing, Quaternary Sci. Rev., 40, 30–38, 2012.
Smith, R. D. and Gent, P. R.: Reference manual for the Parallel Ocean Program (POP), ocean component of the Community Climate Syste Model (CCSM2.0 and 3.0). Technical Report LA-UR-02-2484, Los Alamos National Laboratory, available online at: http://www.ccsm.ucar.edu/models/ccsm3.0/pop, 2002.
Stocker, T. F. and Johnsen, S. J.: A minimum thermodynamic model for the bipolar seesaw, Paleoceanography, 18, 1087, doi:10.1029/2003PA000920, 2003.
Timmermann, A., An, S.-I., Krebs, U., and Goosse, H.: Enso suppression due to weakening of the north atlantic thermohaline circulation, J. Climate, 18, 3122–3139, doi:10.1175/JCLI3495.1, 2005.
Timmermann, A., Okumura, Y., An, S.-I., Clement, A., Dong, B., Guilyardi, E., Hu, A., Junglaus, J. H., Renold, M., Stocker, T. F., Stouffer, R. J., Sutton, R., Xie, S.-P., and Yin, J.: The Influence

CPD
8, 5293–5340, 2012

of a Weakening of the Atlantic Meridional Overturning Circulation on ENSO, J. Climate, 20, 4899–4919, doi:10.1175/JCLI4283.1, 2007a.
Timmermann, A., Lorenz, S. J., An, S.-I., Clement, A., and Xie, S.-P.: The effect of orbital forcing on the mean climate and variability of the tropical Pacific, J. Climate, 20, 4147–4159, doi:10.1175/JCLI4240.1, 2007b.
Tofalo, O., Orgeira, M. J., Compagnucci, R., Alonso, M. S., and Ramos, A.: Characterization of a loess-lapeosols section including a new record of the last interglacial stage in Pampean plain, Argentina, J. S. Am. Eatrh Sci., 31, 81–92, 2011.
Turney, C. S. M. and Jones, R. T.: Does the Agulhas Current amplify global temperatures during super-interglacials?, J. Quaternary Sci., 25, 839–843, 2010.
Tzedakis, P., Frogley, M. R., and Heaton, T. H. E.: Last interglacial conditions in southern Europe: Evidence from Ioannina, northwest Greece, Global Planet. Change, 36, 157–170, 2003.
Vimeux, F., Cuffey, K. M., and Jouzel, J.: New insights into Southern Hemisphere temperature changes from Vostok ice cores using deuterium excess correction, Earth Planet. Sc. Lett., 203, 829–843, doi:10.1016/S0012-821X(02)00950-0, 2002.
Yeager, S. G., Shields, C. A., Large, W. G., and Hack, J. J.: The low-resolution CCSM3, J. Climate, 19, 2545–2566, 2006.
Wang, B. and Fan, Z.: Choice of South Asian summer monsoon indices, B. Am. Meteorol. Soc., 80, 629–638, 1999.
Wang, Y., Cheng, H., Edwards, R. L., Kong, X., Shao, X., Chen, S., Wu, J., Jiang, X., Wang, X., and An, Z.: Millennial and orbital scale changes in the East Asian monsoon over the past 224 000 years, Nature, 451, 1090–1093, 2008.
Xiao, J. L., An, Z. S., Liu, T. S., Inouchi, Y., Kumai, H., Yosihikawa, S. and Kondo,Y.: East Asian mosoon variation during the last 130 000 years evidence from the Loess Plateau of central China and Lake Biwa of Japan, Quaternary Sci. Rev., 18, 147–157, 1999.
Yin, Q. Z. and Berger, A.: Insolation and CO_2 contribution to the interglacial climate before and after the Mid-Brunhes Event, Nature Geosci., 3, 243–246, 2010.
Yin, Q. Z. and Berger, A.: Individual contribution of insolation and CO_2 to the interglacial climates of the past 800 000 years, Clim. Dynam., 38, 709–724, 2012.
Yin, Q., Berger, A., Driesschaert, E., Goosse, H., Loutre, M. F., and Crucifix, M.: The Eurasian ice sheet reinforces the East Asian summer monsoon during the interglacial 500 000 years ago, Clim. Past, 4, 79–90, doi:10.5194/cp-4-79-2008, 2008.

CPD
8, 5293–5340, 2012

Zeng, Z. and Guo, Q.: The relationship between the summer precipitation over Asia- Africa monsoon regions and the tropical easterly jet stream, Chin. J. Atmos. Sci., 6, 283–292, 1982.

Zhao, J.-X., Xia, Q., and Collerson, K. D.: Timing and duration of the Last Interglacial inferred from high resolution U-seris chronology of stalagmite growth in Southern Hemisphere, Earth Planet. Sc. Lett., 184, 635–644, 2001.

CPD

8, 5293–5340, 2012

Table 1. Greenhouse gas concentrations and astronomical parameters used for the PI and the last interglacial simulations in both LOVECLIM and CCSM3.

	Greenhouse gases				Astronomical parameters		
date (kaBP)	CO_2 (ppmv)	CH_4 (ppbv)	N_2O (ppbv)	CO_2eq (ppmv)	eccentricity	obliquity (deg)	longitude perihelion (deg)
0	280	760	270	280	0.01672	23.446	102.04
127	287	724	262	284	0.03938	24.04	275.41

CPD
8, 5293–5340, 2012

Table 2. Mean surface temperature (°C) in LOVECLIM and CCSM3. DJF and JJA stand for December-January-February and June-July-August, respectively.

	Annual		DJF		JJA	
	LOVECLIM	CCSM3	LOVECLIM	CCSM3	LOVECLIM	CCSM3
MIS5	16.5	12.3	13.7	9.6	19.7	15.0
PI	16.0	12.5	14.1	10.8	18.2	14.1
anomaly	0.5	−0.2	−0.4	−1.2	1.4	0.9

CPD
8, 5293–5340, 2012

Table 3. Precipitation anomalies in mm/day, simulated by CCSM3 and LOVECLIM. East Asia summer monsoon (EASM): 20–40° N and 95–145° E; Indian summer monsoon (ISM): 6.5–37.5° N and 67.5–101.5° E; Africa summer monsoon: 0–30° N and 15° W–45° E.

		East Asia	India	Africa
JJA	CCSM3	−0.4	0.75	1.7
	LOVECLIM	0.4	2.05	3.2
DJF	CCSM3	−0.3	−0.32	−0.53
	LOVECLIM	−0.05	−0.23	−0.43

CPD
8, 5293–5340, 2012

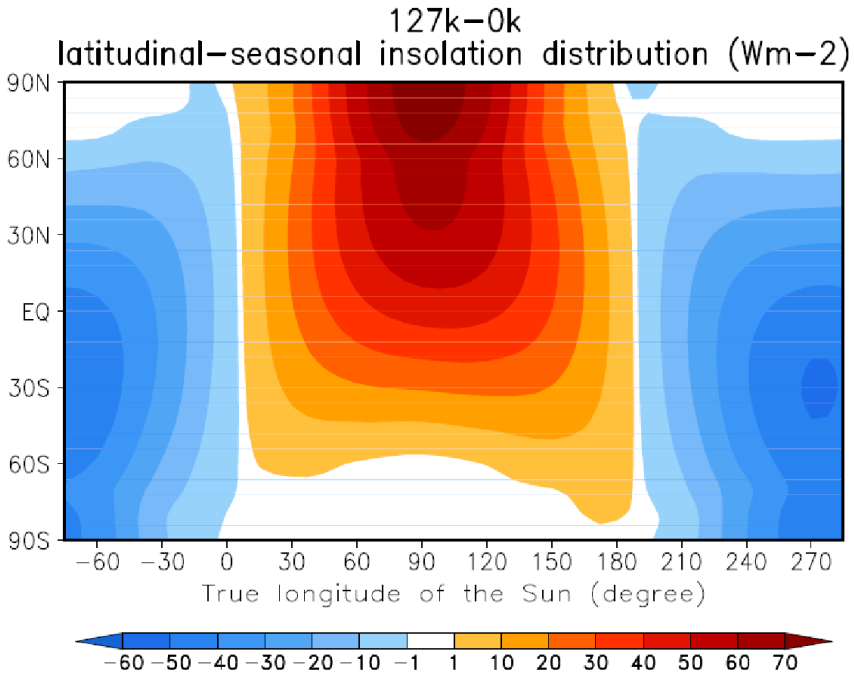

Fig. 1. Difference in the latitudinal-seasonal insolation distribution (Wm^{-2}) between 127 ka BP and PI.

CPD
8, 5293–5340, 2012

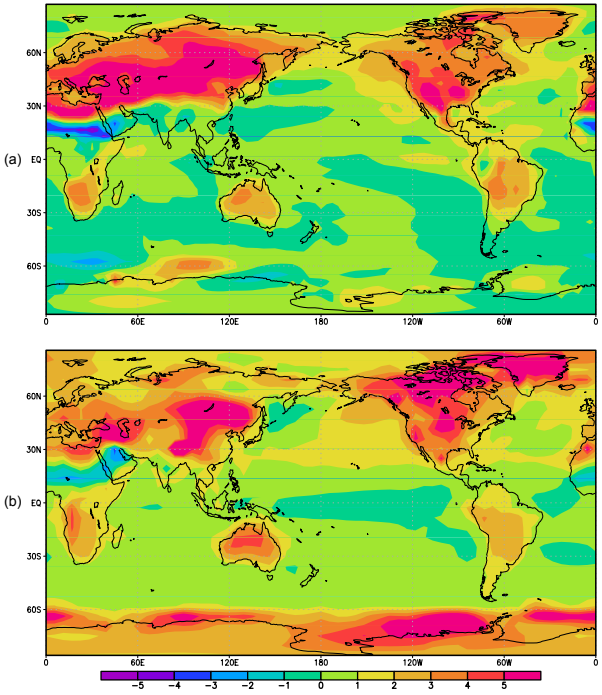

Fig. 2. JJA surface temperature (˚C) anomalies simulated by **(a)** CCSM3 and **(b)** LOVECLIM.

CPD
8, 5293–5340, 2012

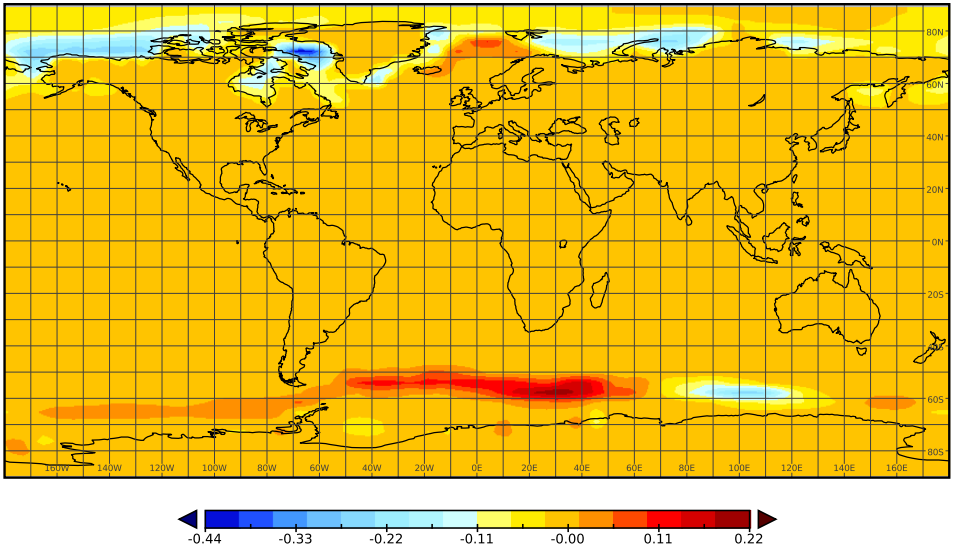

Fig. 3. JJA sea-ice (%) anomaly (MIS5 minus PI) simulated by CCSM3.

CPD
8, 5293–5340, 2012

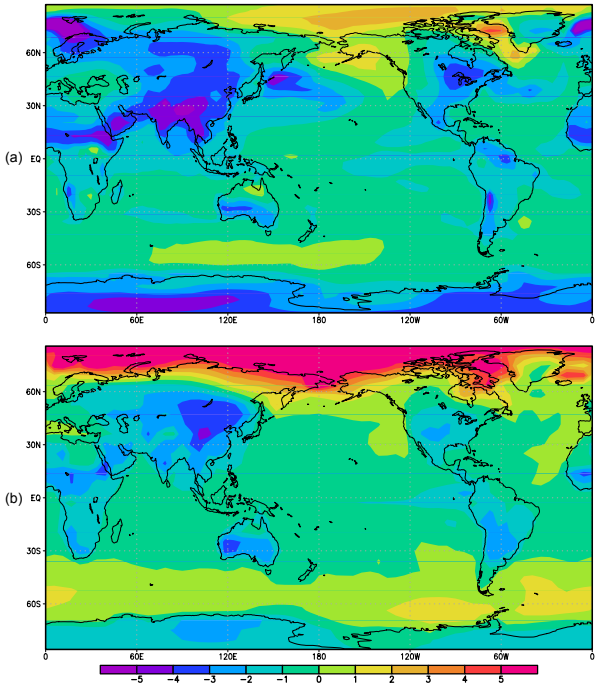

Fig. 4. DJF surface temperature (˚C) anomalies simulated by **(a)** CCSM3 and **(b)** LOVECLIM.

CPD
8, 5293–5340, 2012

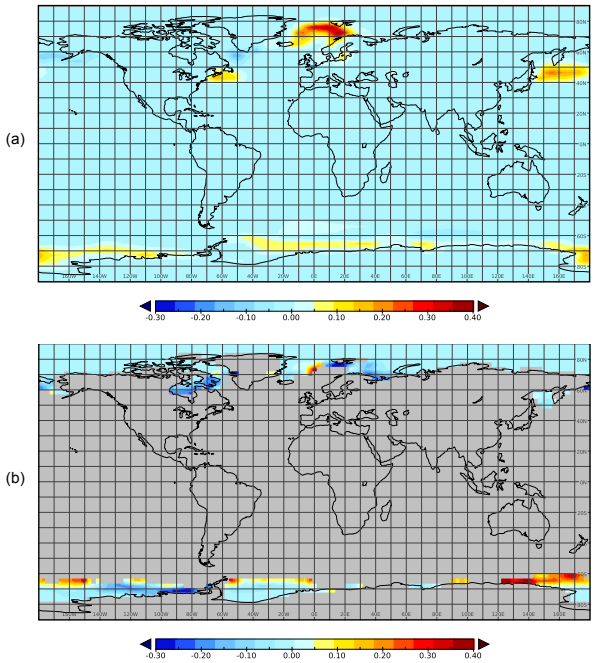

Fig. 5. DJF sea-ice (%) anomalies simulated by **(a)** CCSM3 and **(b)** LOVECLIM.

CPD
8, 5293–5340, 2012

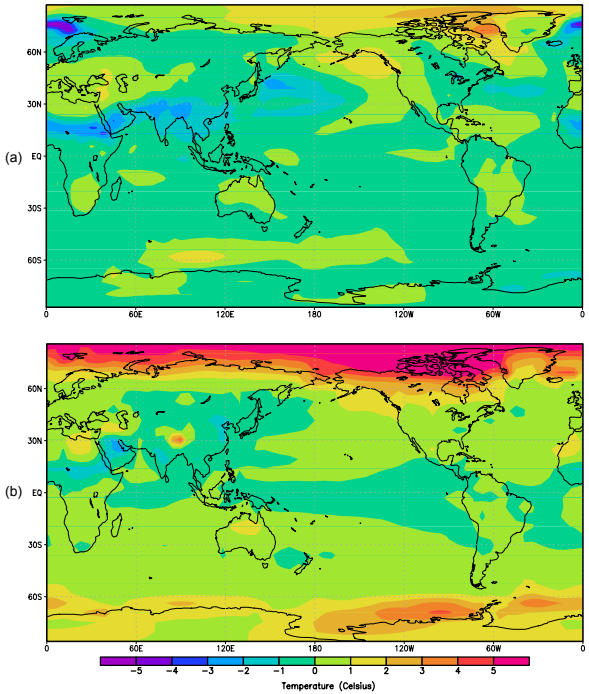

Fig. 6. Annual surface temperature (°C) anomalies simulated by **(a)** CCSM3 and **(b)** LOVECLIM.

CPD
8, 5293–5340, 2012

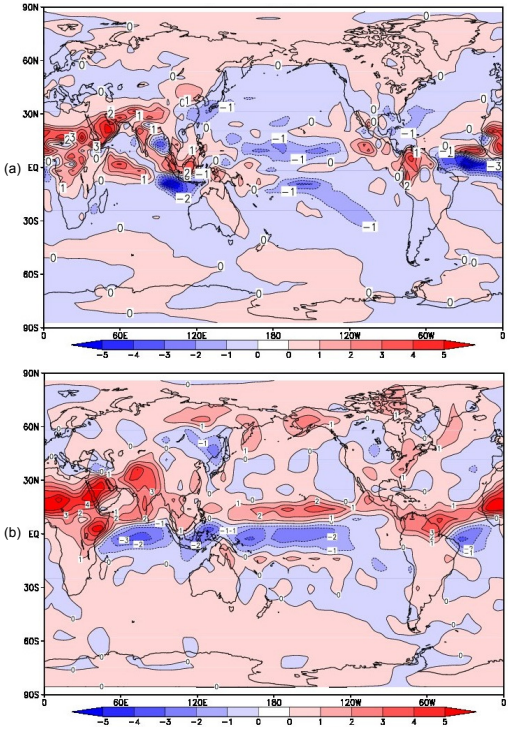

Fig. 7. JJA precipitation (mm day^{-1}) anomalies simulated by **(a)** CCSM3 and **(b)** LOVECLIM.

CPD
8, 5293–5340, 2012

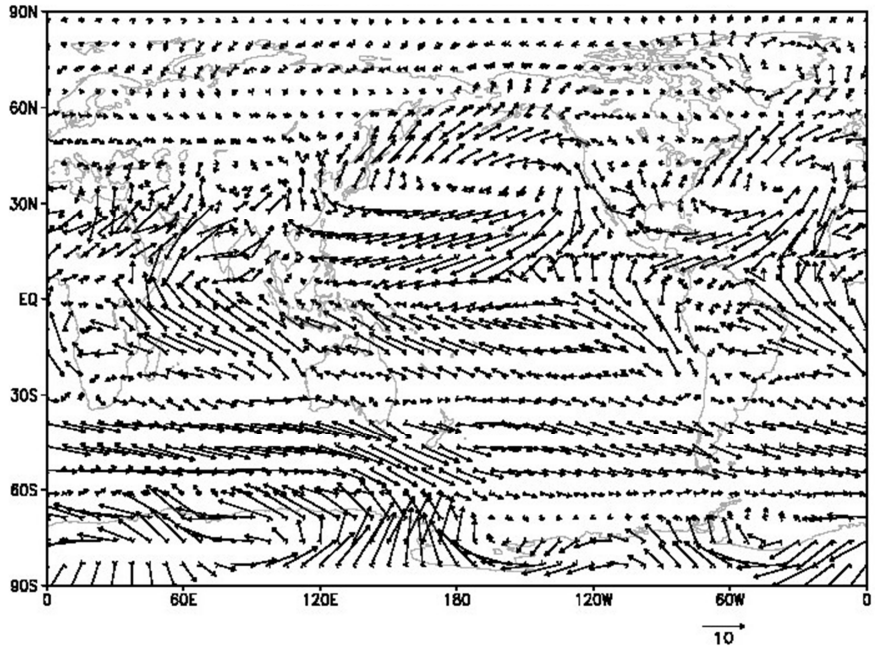

Fig. 8. JJA surface wind ($m\,s^{-1}$) anomaly in CCSM3.

CPD
8, 5293–5340, 2012

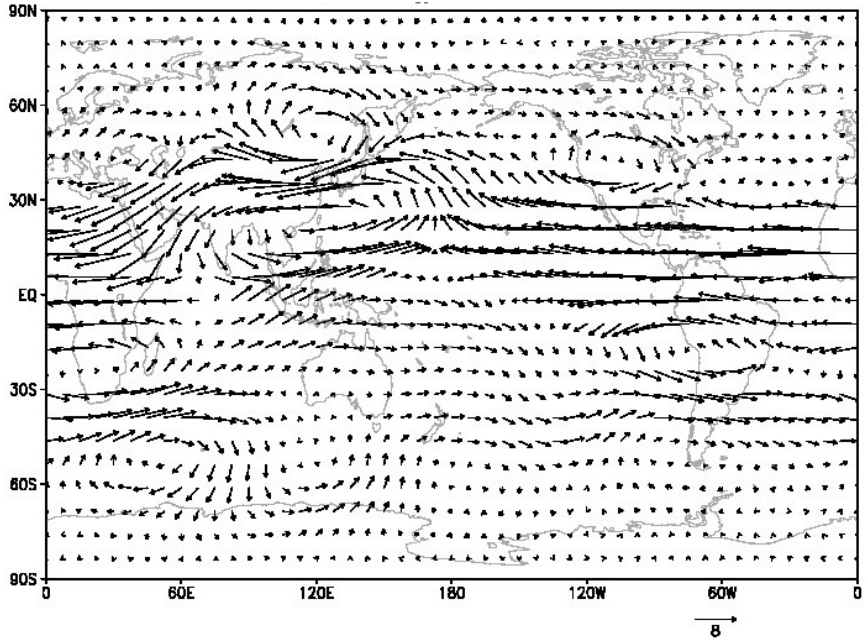

Fig. 9. Tropical Easterly Jet ($m\,s^{-1}$) anomaly in CCSM3.

CPD
8, 5293–5340, 2012

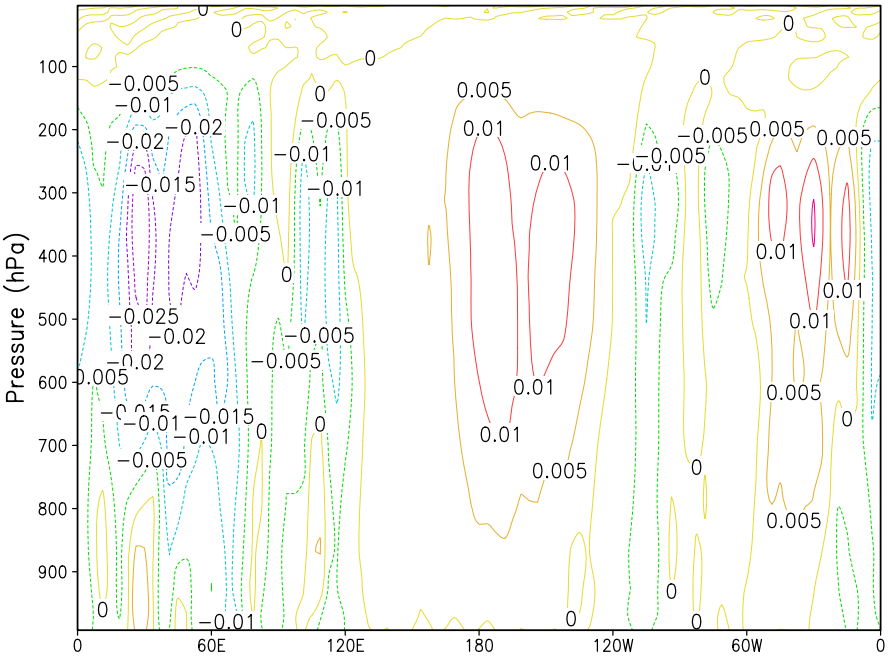

Fig. 10. Vertical velocity (Pa s^{-1}) simulated in CCSM3.

CPD
8, 5293–5340, 2012

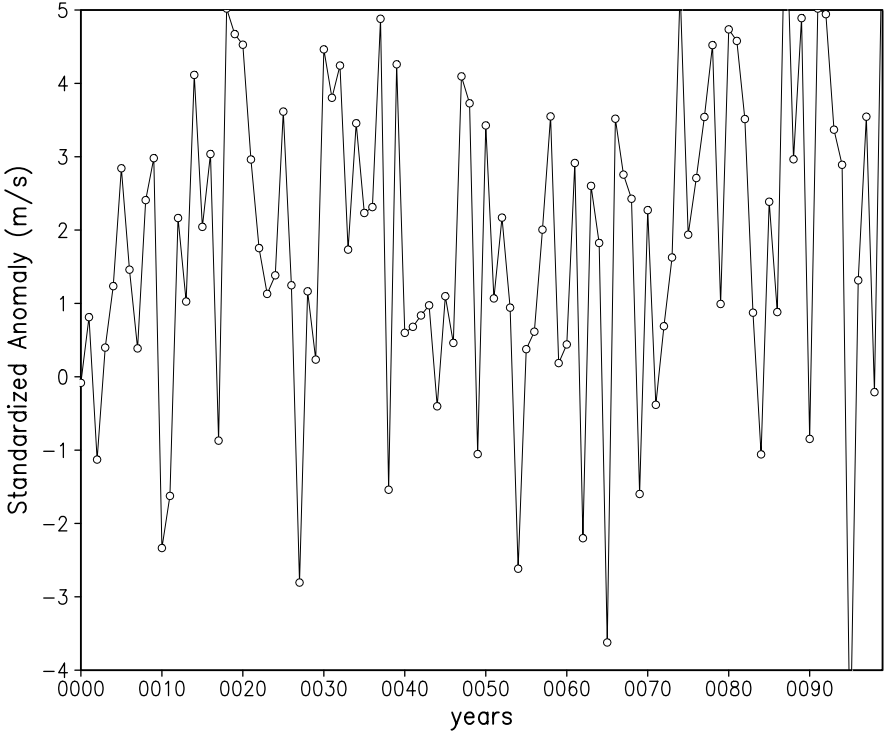

Fig. 11. IMI index in CCSM3 (MIS5 minus PI).

CPD
8, 5293–5340, 2012

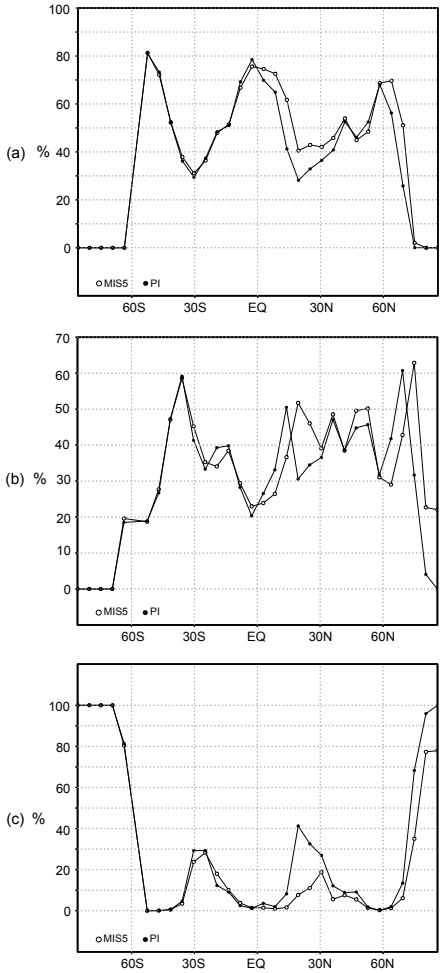

Fig. 12. Vegetation fraction (%) simulated by LOVECLIM for **(a)** trees; **(b)** grass and **(c)** desert.

CPD
8, 5293–5340, 2012




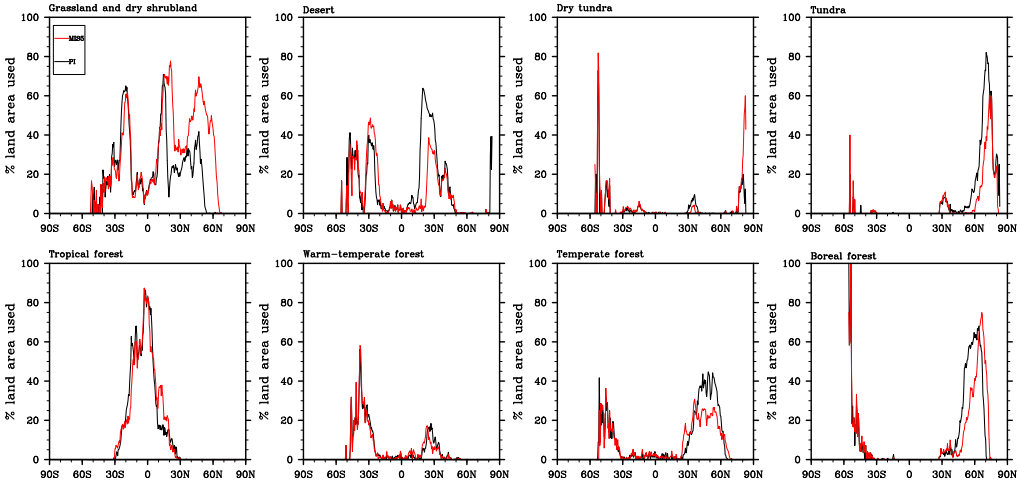

Fig. 13. Vegetation fraction (%) simulated in BIOME4.

CPD
8, 5293–5340, 2012

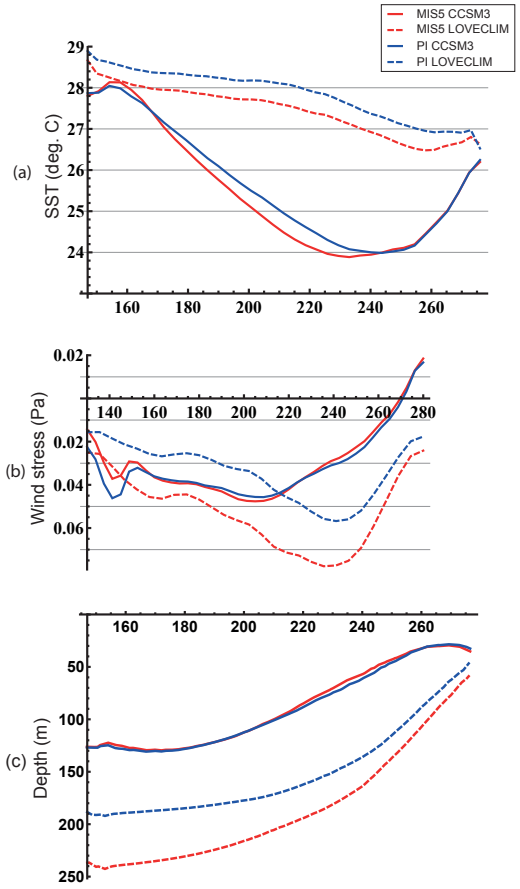

Fig. 14. LOVECLIM and CCSM3 simulations of **(a)** SST (°C); **(b)** wind stress (Pa) and **(c)** depth of the thermocline (m). x-axis indicates longitude in ° E.

CPD
8, 5293–5340, 2012

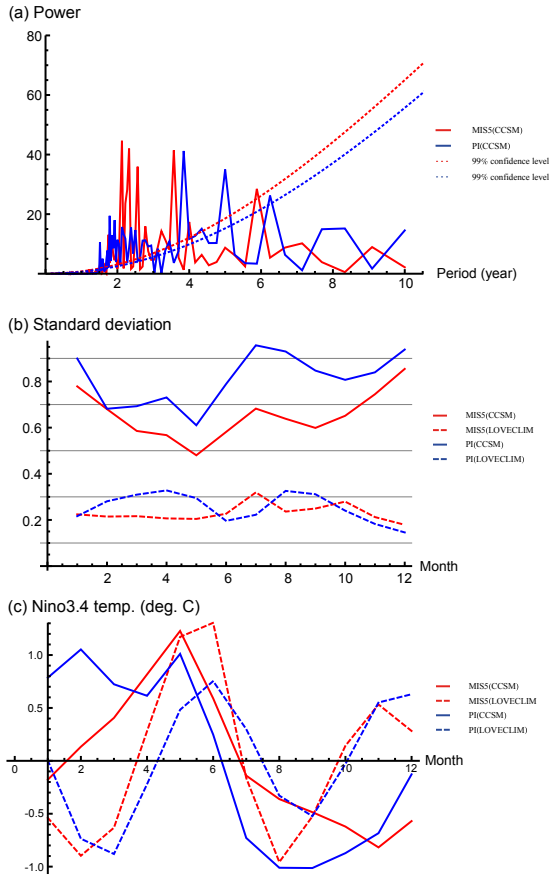

Fig. 15. LOVECLIM and CCSM3 results for **(a)** spectrum for SST anomalies; **(b)** monthly standard deviation for SST anomalies and **(c)** monthly SST anomalies.

CPD
8, 5293–5340, 2012